Transition Metal Ion-Based Nanocrystalline Luminescent Thermometry in SrTiO3:Ni2+,Er3+ Nanocrystals Operating in the Second Optical Window of Biological Tissues

C. Matuszewska, K. Elzbieciak-Piecka, L. Marciniak

THE JOURNAL OF PHYSICAL CHEMISTRY C

Article

Cite This: J. Phys. Chem. C XXXX, XXX, XXX−XXX

pubs.acs.org/JPCC

Transition Metal Ion-Based Nanocrystalline Luminescent Thermometry in $SrTiO_3:Ni^{2+},Er^{3+}$ Nanocrystals Operating in the Second Optical Window of Biological Tissues

C. Matuszewska, K. Elzbieciak-Piecka, and L. Marciniak*

Institute of Low Temperature and Structure Research, Polish Academy of Sciences, Okólna 2, 50-422 Wroclaw, Poland

Supporting Information

ABSTRACT: Luminescence thermometry in the second and third optical windows of biological tissues has gained importance in recent years due to the reduction of both absorption and scattering effects in human tissues, which substantially increase its applicative potential. In this work, we present a luminescent thermometer based on $SrTiO_3:Ni^{2+},Er^{3+}$ nanocrystals, which is the first reported study of nanothermometry based on Ni^{2+} ion luminescence. The $SrTiO_3:Ni^{2+},Er^{3+}$ nanocrystals were successfully synthesized using the Pechini method. The spectroscopic properties of obtained nanocrystals were investigated in a wide temperature range, namely, between −150 and 210 °C. It was found that Ni^{2+} ions in the $SrTiO_3$ matrix are characterized by broadband emission localized in the II optical window at about 1200 nm, which additionally changes its spectral position toward longer wavelengths with the rise of temperature. Three temperature-dependent parameters were studied for luminescence thermometry: changes in the emission intensity of the Ni^{2+} band, the spectral shift of its maximum, and the luminescence intensity ratio of Ni^{2+} to Er^{3+} ions. The temperature-sensing properties of $SrTiO_3:Ni^{2+},Er^{3+}$ were investigated as a function of Er^{3+} concentration. It was revealed that the increase of thermal sensitivity was associated with the decrease of Er^{3+} concentration. The highest value of the relative sensitivity, in the physiological temperature range, was obtained for $SrTiO_3$:0.05% Ni^{2+},0.1% Er^{3+} nanocrystals, namely, 0.80%/°C at 40 °C.

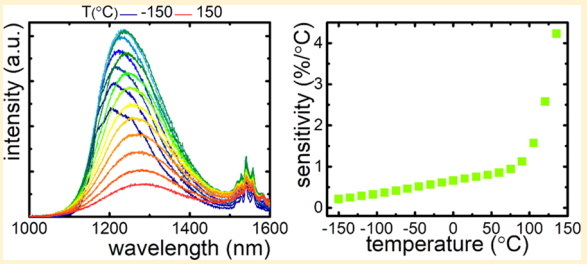

INTRODUCTION

Temperature is one of the most fundamental thermodynamic parameters that affects a vast number of physical processes as well as chemical reactions.[1] Moreover, it determines the dynamics and structure of biological systems, notably cell division rates and tissue growth as a consequence.[2] Monitoring temperature with high sensitivity and submicrometric spatial resolution is crucial for early detection and the effective treatment of many diseases such as cancer, stroke, or inflammation process.[3,4] To understand and control these processes, the ability of a fast, accurate, and precise way of temperature determination is needed to be provided. Nowadays, disparate methods of temperature measurement are available, as follows: based on volume expansion, pressure, resistance thermometers, and IR cameras to mention just a few. Nevertheless, one of the most important issues related to the conventional thermometers is their contact operating mode that makes temperature readout, i.e., in the case of biological systems, impossible. The IR cameras are able to operate in the noncontact mode; however, they provide information only about the temperature distribution on the surface of the tissue, which, as it was proved by Jaque et al.,[5] may significantly differ from the real temperature of the nanoparticles localized below the skin. On the other hand, luminescence thermometry is a technique that takes advantage of the temperature-dependent luminescent features of the phosphor for temperature determination and therefore may be an important alternative for conventional measurement methods.[6,7] Nowadays, luminescence nanothermometry (LNTh) is the only noncontact method providing the resolution and sensitivity required for effective in vivo and in vitro temperature measurement in biosystems.[3,4]

Due to the very complex structures of animal and human tissues, which comprise of disparate components differing in size, shape, and chemical composition, it is particularly tough to provide effective light interaction with turbid media.[3] In medical diagnosis and treatment, one of the most important parameters is the depth of light penetration that depends on the energy of the incident light. It has been proven that both absorption and scattering increase when the photon energy has intensified.[3,8,9] However, there are specific regions in the near-infrared spectral range, where the level of absorption and scattering is minimal, termed "optical windows" (OW) that are especially usable in medical treatment and diagnosis (I OW, 650−950 nm; II OW, 1000−1350 nm; and III OW, 1550−1870 nm).[3,10]

There are numerous examples of materials emitting in the I OW window that can be potentially used in LNThs.[11,12]

Received: April 29, 2019
Revised: June 5, 2019
Published: July 5, 2019

DOI: 10.1021/acs.jpcc.9b04002
J. Phys. Chem. C XXXX, XXX, XXX−XXX

However, the use of the II OW can be more beneficial for biomedical application, in contrast to the I OW, as it lowers the intensity of autofluorescence of tissues and, due to lower absorption and scattering of light by the tissue, improves the penetration depth in this spectral range. Nevertheless, exploitation of II and III OWs for sustained periods has been hindered by a lack of proper luminescent materials and sensitive detectors in the NIR region.[13−15] Advancements in technology mean the application of II and III OWs in LNTh has gained much attention, owing to the fact that it can provide noticeable improvements in depth of imaging and image contrast. Moreover, as it was recently proved, the maximum obtained value of the relative sensitivity in the II OW in the case of some phosphors like nanoperovskites is twice higher in respect to the I OW counterpart.[16] Recent reports on materials emitting in the II OW with temperature-dependent luminescence mainly focus on singly and doubly rare earth-doped nanoluminophores.[16−18] Cerón et al. have put forward different approaches by combining $NaGdF_4$:Nd^{3+} nanocrystals with semiconductor PbS/CdS/ZnS quantum dots in a hybrid nanostructure formed by poly(lactic-*co*-glycolic acid) (PLGA).[19] However, semiconductor quantum dots comprised of highly toxic compounds, along with considerably large sizes (over 100 nm), hider their in vivo applications.[13,20] A very promising alternative has been introduced by Ruiz et al. who used Ag/Ag_2S nanocrystals that provide remarkable thermal sensitivity up to 4%/°C, and additionally, this material is characterized by low cytotoxicity and excellent heating properties upon optical excitation.[20]

In our approach, we focus on the luminescence of nanocrystalline inorganic materials codoped with lanthanide metal (Ln^{3+}) ions and transition metal (TM) ions. Since the luminescence thermal quenching of the Ln^{3+} ion, due to the lack of intersection point between ground and excited states, is mainly governed by the multiphonon processes, its emission presents relatively low thermal quenching and therefore it can be exploited as a reference to significantly more susceptible to temperature changes of the TM ion.[11,21] In that case, the parameter used to determine temperature is the ratio of the emission bands of these two ions.[4,15] So far, a few TM ions have been exploited in LNTh using the approach mentioned above, as follows: Cr^{3+},[22−26] Mn^{4+}, Mn^{3+},[27−3227−32] V^{3+}, V^{4+}, V^{5+},[33,34] Ti^{4+}, Ti^{3+},[35] and Co^{2+}.[3636] However, their use is currently limited to the I OW, which, compared to the II and III OW, is less favorable in terms of biomedical applications.

In this work, we introduce, for the first time, a nanocrystalline bandshape luminescent thermometer based on the TM emission intensity emitting in the II OW spectral range, $SrTiO_3$:Ni^{2+},Er^{3+} nanocrystals. Ni^{2+} is distinctively suited for the II OW because of broadband emission in the NIR region of octahedrally coordinated ions embedded in the nanocrystalline host. Its spectroscopic properties are the result of incompletely filled d shells, providing numerous energy levels in between which d−d optical transitions may occur. Owing to the fact that 3d electrons participate in bond creation, all TM ions are highly susceptible to local symmetry changes.[11,15] To date, Ni^{2+}-doped glasses and ceramics have been used as an active media in tunable lasers, broadband amplifiers, solar cells, novel display technologies, and high-density optical storage and infrared sensors due to their excellent optical properties.[37,38] However, its ability of noncontact temperature sensing has never been investigated, on the contrary to Er^{3+} ions, in which green emission has already been exploited for the aim of luminescence thermometry.[39−41] Introducing Ni^{2+} ions to the nanocrystalline matrix enables us to exploit the spectral range of the II OW, much more favorable in terms of medicine due to reduced autofluorescence and scattering effects in tissues, which is a significant advancement compared to the previously used TM ions. Therefore, in this paper, spectroscopic properties of $SrTiO_3$:Ni^{2+},Er^{3+} nanocrystals of different grain sizes and dopant concentrations were comprehensively investigated in a wide temperature range with special emphasis on the verification of their applicative potential in luminescence thermometry.

EXPERIMENTAL SECTION

Synthesis. $SrTiO_3$:Ni^{2+},Er^{3+} nanocrystals were successfully synthesized using a modified Pechini method.[42] $Sr(NO_3)_2$ (strontium nitrate, Puratronic, 99.9965% purity), $Ni(NO_3)_2 \cdot 6H_2O$ (nickel(II) hexahydrate, Puratronic, 99.9985% purity), Er_2O_3 (erbium oxide, Sigma-Aldrich, 99.999% purity), $Ti[O(CH_2)_3CH_3]_4$ (titanium(IV) *n*-butoxide, Alfa Aesar, >99% purity), $C_6H_8O_7$ (citric acid, anhydrous, Alfa Aesar, >99.5% purity), $H(OCH_2CH_2)_nOH$ (poly(ethylene glycol), 200, Alfa Aesar), and $C_5H_8O_2$ (2,4-pentanedione, Alfa Aesar, 99% purity) were used as starting materials. Stoichiometric amounts of strontium nitrate and nickel(II) hexahydrate were dissolved in deionized water in separate glasses and then mixed together. Erbium oxide was dissolved in deionized water with addition of small amount of nitric acid, recrystallized three times, and added to the water solution of strontium and nickel ions. Titanium butoxide was dissolved in 2,4-pentanedion to prevent its hydrolysis and added to the water solution of nitrates. Citric acid was dissolved in deionized water at 50 °C and combined with previously obtained emulsion, which was then left for mixing for 30 min. Subsequently, poly(ethylene glycol) was added and all substrates have been mixed for 2 h. The obtained sol was then dried at 90 °C for 7 days and annealed at 850 °C for 8 h. To analyze the influence of Ni^{2+} concentration on the spectroscopic properties of the strontium perovskite, seven samples were prepared with Ni^{2+} mol concentration changed in the range from 0.01 to 1.0%. All concentrations presented in this work are intentional and are calculated in respect of Ti^{4+} ions.

Powder diffraction studies were carried out on a PANalytical X'Pert Pro diffractometer equipped with an Anton Paar TCU 1000 N temperature control unit using Ni-filtered Cu Kα radiation (V = 40 kV, I = 30 mA).

Transmission electron microscopy images were obtained using an FEI Tecnai G2 20 S/TEM microscope. The microscope was equipped with a thermionic LaB6 emitter and an EDS detector for elemental analysis. The study was conducted in the TEM mode at a maximum voltage of 200 kV. Micrographs were taken at various magnifications, including high-resolution images with lattice fringes.

The emission spectra were measured using the 375 nm excitation line from a laser diode and measured using an Edinburgh Instruments FLS980 fluorescence spectrometer (0.2 nm spectral resolution). The measurements were carried out with a R5509-72 Hamamatsu photomultiplier cooled with liquid nitrogen for the NIR spectral range. The temperature of the sample was controlled using a Linkam THMS 600 heating stage (0.1 °C temperature stability and 0.1 °C set point resolution).

The excitation spectra were obtained using an Edinburgh Instruments FLS980 fluorescence spectrometer. The measure-

DOI: 10.1021/acs.jpcc.9b04002
J. Phys. Chem. C XXXX, XXX, XXX−XXX

ments were carried out with a 450 W xenon lamp and two detectors, a Hamamatsu R928P side window photomultiplier in the visible spectral range and a Hamamatsu R5509-72 photomultiplier cooled with liquid nitrogen for the NIR spectral range.

RESULTS AND DISCUSSION

The $SrTiO_3$ nanocrystals belong to the structural family of ABX_3 perovskites that crystallizes in the cubic structure of the $Pm\bar{3}m$ space group (a = 3.8947 Å).[43] Their structure consists of TiO_6 octahedrons with Sr^{2+} ions occupying 12-fold coordinated sites surrounded by eight such octahedrons, as presented in Figure 1a. However, it is rare to obtain such an ideal structure; in fact, most mineral perovskites crystallize in a slightly distorted "pseudocubic" structure. Cubic $SrTiO_3$ exhibits three phase transitions upon cooling from room temperature, resulting in a tetragonal phase (−210 to −160 °C), an orthorhombic phase (−240 to −220 °C), and possibly a rhombohedral phase (below −260 °C).[43,44] The average Ti^{4+}−O^{2-} bond length is 1.952 Å. Ni^{2+} ions are able to occupy tetrahedral as well as octahedral sites; however, emission is only possible to obtain while occupying the latter. Due to comparable effective ionic radii (CN, coordination number; $R_{Ti^{4+}(CN=6)}$ = 74.5 pm, $R_{Ni^{2+}(CN=6)}$ = 83.0 pm, $R_{Sr^{2+}(CN=8)}$ = 140 pm, and $R_{Er^{3+}(CN=8)}$ = 114.4 pm),[45] in this host material, Ni^{2+} ions substitute octahedral sites of 6-fold coordinated Ti^{4+} ions, while Er^{3+} ions substitute that of 12-fold coordinated Sr^{2+} ions.

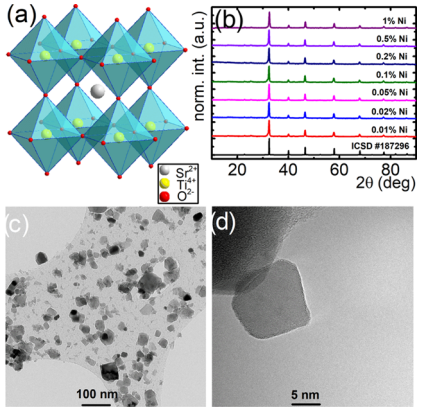

Figure 1. Structure and morphology of $SrTiO_3$:Ni^{2+} nanocrystals: structure visualization of $SrTiO_3$ matrix (a), X-ray diffraction (XRD) patterns of $SrTiO_3$:Ni^{2+} nanocrystals for different Ni^{2+} ion concentrations (b), and representative TEM images of $SrTiO_3$:1% Ni^{2+} nanocrystals (c, d).

Implementation of Ni^{2+} ions may cause distortions in the crystalline matrix since the ionic radius of Ni^{2+} is slightly larger than the ionic radius of Ti^{4+} and can result in lowering the symmetry, which can occur additionally with lowering the temperature. Owing to low concentrations of Ni^{2+}, its substitution for Ti^{4+} ions did not generate any phase modulation in the case of our nanocrystals. The crystallographic purity of the synthesized nanocrystalline material was confirmed by XRD measurements (Figure 1b). Each of the diffraction peaks obtained from the XRD measurements matches the reference pattern (ICSD 187296), and the concentration of Ni^{2+} ions has no influence on the purity of the crystalline phase. The characteristic broadening of diffraction peaks is due to the nanometric size of crystals. The grain size as well as unit cell parameters for rising concentrations of Ni^{2+} ions shows no visible tendency. The XRD measurements of $SrTiO_3$:Ni^{2+},Er^{3+} (Figure S1) proved, furthermore, that charge imbalance caused by the substitution of a divalent Sr^{2+} with a trivalent Er^{3+} did not generate any secondary phases, and therefore, addition of alkali ions for charge compensation was dispensable. The characteristic increase of the grain size from 31 to 46 nm with the annealing temperature (changed from 850 to 1100 °C) was confirmed; however, when it comes to unit cell parameters, no tendency

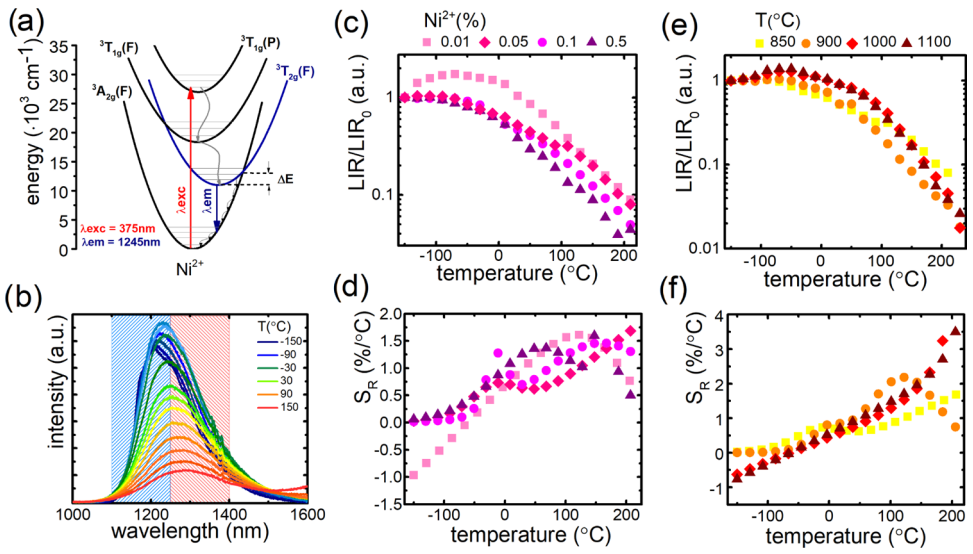

Figure 2. Spectroscopic characterization of $SrTiO_3$:Ni^{2+} nanocrystals: schematically presented energy-level diagram of Ni^{2+} ions in the $SrTiO_3$ structure (a); emission spectra of $SrTiO_3$:0.01% Ni^{2+} nanocrystals as a function of temperature (b); comparison of normalized integral intensities for different concentrations of Ni^{2+} ions in the $SrTiO_3$ structure annealed at 850 °C as a function of temperature (c); comparison of relative sensitivity for different concentrations of Ni^{2+} ions in the $SrTiO_3$ structure annealed at 850 °C as a function of temperature (d); comparison of normalized integral intensities for different annealing temperatures of $SrTiO_3$:0.05% Ni^{2+} nanocrystals as a function of temperature (e); and comparison of relative sensitivities for different annealing temperatures of $SrTiO_3$:0.05% Ni^{2+} nanocrystals as a function of temperature (f).

DOI: 10.1021/acs.jpcc.9b04002
J. Phys. Chem. C XXXX, XXX, XXX−XXX

was found. The XRD measurements of nanocrystals annealed at higher temperatures are presented in Figure S2. The representative TEM images, presented in Figure 1c,d, depict that synthesized powders consist of grains relatively well separated from each other, which do not form massive aggregates. Moreover, Figure 1d confirms the high crystallinity of obtained grains.

To fully understand processes of light interaction with obtained $SrTiO_3$:Ni^{2+} nanocrystals, knowledge of electronic transitions occurring between the ground state and disparate excited state is essential. Strong dependence of the crystal field strength of the matrix on spectroscopic properties of 3d ions has outright reflexion in energy-level diagrams (Figure 2a). Spectroscopic properties of $SrTiO_3$:Ni^{2+} nanocrystals have been investigated under 375 nm excitation, which provides transition of electrons from the $^3A_{2g}(F)$ ground state to the $^3T_{1g}(P)$ excited state. Apart from broadband emission of Ni^{2+} ions in the NIR region, no other emission band characteristic for these ions has been revealed in the VIS region of the spectrum. This suggest that after excitation to the $^3T_{1g}(P)$ state nonradiative relaxation processes lead to the population of the $^3T_{1g}(F)$ state. Occurrence of an intersection point between $^3T_{2g}(F)$ excited state and $^3A_{2g}(F)$ ground state parabolas at the ΔE energy (see Figure 2a) determines thermal quenching of Ni^{2+} ion luminescence.

A thorough investigation of emission spectra was conducted over a wide range of temperature (−150 to 210 °C) to fully understand luminescence thermal quenching processes in this material. Figure 2b presents emission spectra of the $SrTiO_3$:0.01% Ni^{2+} nanocrystals as a function of temperature. Emission spectra of Ni^{2+} ions comprise a broad band centered at around 1250 nm, which is associated with the $^3T_{2g}(^3F) \rightarrow {}^3A_{2g}(^3F)$ transition. It can be noticed that the spectral position of the band's maximum shifts toward longer wavelengths (red shift) from 1206 nm at −150 °C to 1286 nm at 150 °C, which suggests that a rise in temperature results in distortion of Ni^{2+} energy levels. Its intensity initially increases with temperature, reaching a maximum value at −70 °C and thermally quenches afterward, with total suppression at around 200 °C. The initial rise of emission intensity might be associated with the fact that the excitation line reaches the side of the absorption band and therefore during temperature increase the effective cross section of absorption rises, resulting in stronger emission. When the provided thermal energy overcomes the activation energy, the nonradiative depopulation of the $^3T_{2g}(^3F)$ state becomes efficient. Therefore, as a result, thermal quenching of emission occurs. The calculated activation energy for $SrTiO_3$:0.01% Ni^{2+} was around 2140 cm^{-1}, and this value varies irregularly with concentration and annealing temperature (the procedure for calculating the value of activation energy is presented in the Supporting Information).

The integral intensity as the function of temperature for different dopant concentrations is illustrated in Figure 2c. The thermal quenching tendency is similar for nanocrystals doped with three higher concentrations, the most effective achieved for 0.5% Ni^{2+}, while the nanocrystals with the lowest concentration present an initial rise of integral intensity. This increase is associated with the fact that excitation wavelength hits the sideband of the Ni^{2+} absorption band. Therefore, an increase in the temperature causing the broadening of the absorption band leads to the more efficient absorption of the excitation wavelength. The broadening of the absorption band is also caused by the number of optically active ions localized in the nonequivalent crystallographic sites, i.e., strongly distorted surface sites. Hence, the most spectacular rise of the emission intensity was observed in the case of the lowest dopant concentration. The rate of the quenching process can be expressed by the relative sensitivity of luminescent thermometers according to the following formula

$$S_R = \frac{1}{A}\frac{\Delta A}{\Delta T} \times 100\% \quad (1)$$

where A is a temperature-dependent parameter (in this case, the value of integral intensity of the Ni^{2+} emission band in the range of 1150−1200 nm is normalized to the first value at −150 °C), while ΔA expresses the change of A related to the change of temperature, ΔT. The highest value of the relative sensitivity was found to be S_R = 1.48%/°C at 120 °C; however, in the physiological temperature range, the values of the S_R were comparable for each of the Ni^{2+} concentration (Figure 2d). The maximal value of S_R = 0.82%/°C at 30 °C was found for Ni^{2+} = 0.5%. However, due to the concentration quenching of emission intensity, the overall emission observed for this sample is significantly lower in respect to that of the 0.05%. Therefore, Ni^{2+} concentration of 0.05% was selected for further analysis.

In the case of each grain size, initially at low temperatures, the rise of the Ni^{2+} emission intensity can be observed up to around 0 °C, above which a gradual quenching of its intensity appears. For bigger grain sizes, the contribution of the surface ions to the overall emission intensity is smaller. Therefore, for bigger nanoparticles, absorption bands are usually much narrower in respect to those of the smaller ones. As a consequence, the broadening of the absorption band at higher temperatures leads to a greater increase of emission intensity, as can be seen in Figure 2e. Observed differences are quantitatively expressed by the thermal evolution of S_R, as shown in Figure 2f. In low (below 0 °C) and high (above 100 °C) temperature ranges, the influence of the nanoparticle size (modulated by the annealing temperature) on the S_R is the most spectacular. However, in the physiological temperature range, obtained values of S_R are almost independent of the particle size. The fact that the Ni^{2+} emission band maximum undergoes spectral shift with temperature can be used for a noncontact temperature readout. Therefore, the luminescence intensity ratio (LIR_1) parameter is defined as follows

$$LIR_1 = \frac{\int I(1100-1250\ \text{nm})}{\int I(1250-1400\ \text{nm})} \quad (2)$$

Mentioned spectral ranges are denoted as blue and red regions in Figure 2b, and calculated thermal evolutions of LIR_1 and S_R are shown in Figures S3 and S4. In this approach, obtained values of relative sensitivity reached a maximum value of S_R = 0.25%/°C in the physiological temperature range. Presented calculations indicate that for $SrTiO_3$:Ni^{2+} nanocrystals a luminescent thermometer based on the overall emission intensity provides a more sensitive temperature readout.

As it is well known that the absolute emission intensity of a particular emission band of the phosphor is dependent on many experimental conditions including the excitation density, distance, angle between the phosphor and the detection system, etc. Therefore, to improve the reliability of a noncontact temperature readout, a ratiometric technique should be implemented. To accomplish this, the Er^{3+} ions

DOI: 10.1021/acs.jpcc.9b04002
J. Phys. Chem. C XXXX, XXX, XXX−XXX

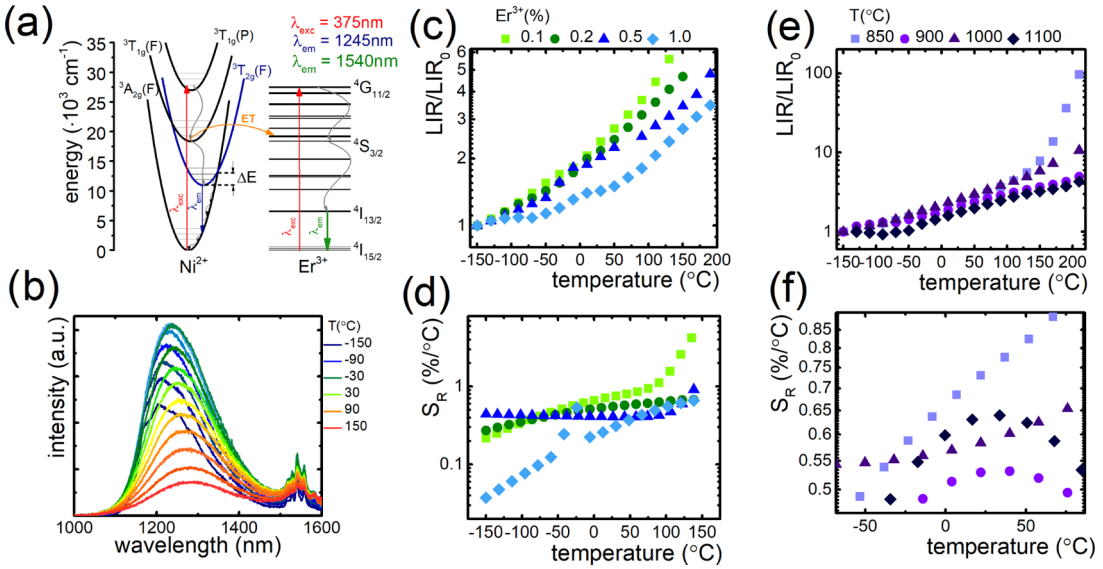

Figure 3. Spectroscopic characterization of $SrTiO_3$:Ni^{2+},Er^{3+} nanocrystals: schematically presented energy-level diagram of Ni^{2+} and Er^{3+} ions in the $SrTiO_3$ structure (a); emission spectra of $SrTiO_3$:0.05% Ni^{2+},0.1% Er^{3+} nanocrystals as a function of temperature (b); comparison of the normalized LIR value for different concentrations of Er^{3+} ions in the $SrTiO_3$:0.05% Ni^{2+},Er^{3+} structure annealed at 850 °C as a function of temperature (c); comparison of the relative sensitivity for different concentrations of Er^{3+} ions in the $SrTiO_3$:0.05% Ni^{2+},Er^{3+} structure as a function of temperature (d); comparison of the normalized LIR value for different annealing temperatures of $SrTiO_3$:0.05% Ni^{2+},0.1% Er^{3+} nanocrystals as a function of temperature (e); and comparison of the relative sensitivity for different annealing temperatures of $SrTiO_3$:0.05% Ni^{2+},0.1% Er^{3+} nanocrystals as a function of temperature (f).

were introduced to the $SrTiO_3$:Ni^{2+} nanocrystals as a codopant, emission of which can be used as a luminescence reference. According to our previous studies, the appropriate selection of excitation wavelength (which simultaneously excites both types of optically active ions) enables us to enhance the relative sensitivity of the luminescent thermometer.[11] Therefore, excitation spectra for all concentrations of Er^{3+} were measured by monitoring the $^4I_{13/2} \rightarrow {}^4I_{15/2}$ emission band at 1530 nm (Figure S2). From these spectra, it can be clearly seen that the UV/blue spectral range should be the most suitable to fulfill these requirements. Since radiation from UV as well as visible spectral range is not desirable in terms of biomedical applications, engineering a matrix in which both excitation and emission bands are localized within the ranges of optical windows of biological tissues will be the main objective of further investigations. The most characteristic absorption band of Er^{3+} ions is related to the $^4I_{15/2} \rightarrow {}^4G_{11/2}$ absorption band at 375 nm. However, in the case of $SrTiO_3$:Ni^{2+},Er^{3+} ions, the $^3A_{2g}(F) \rightarrow {}^3T_{1g}(P)$ band of Ni^{2+} dominates over $^4I_{15/2} \rightarrow {}^4G_{11/2}$. Therefore, the independent excitation of each of the ions is strongly limited in this host material and hence the $Ni^{2+} \rightarrow Er^{3+}$ energy transfer provides an efficient population channel of Er^{3+} ion excited states. This is an important fact since the decrease of the Ni^{2+} emission intensity may lower the Er^{3+} intensity, which is used as a reference signal in our approach, and as a consequence may hinder the relative sensitivity of the luminescent temperature sensor. The energy diagram for these two ions is presented in Figure 3a. As can be clearly seen, λ_{exc} of 375 nm enables to excite Er^{3+} ions through the $^4I_{15/2} \rightarrow {}^4G_{11/2}$ electronic transition, which followed by the nonradiative de-excitation populates the $^4I_{13/2}$. Radiative depopulation of this state through the $^4I_{13/2} \rightarrow {}^4I_{15/2}$ electronic transition leads to the generation of an intense band at 1.55 μm. The characteristic broadband emission of Ni^{2+} ions at around 1.25 μm is ascribed to the $^3T_{2g}(F) \rightarrow {}^3A_{2g}(F)$ transition. As a result, the emission spectra of $SrTiO_3$:0.05% Ni^{2+},0.1% Er^{3+} measured over a wide range of temperature (−150 to 210 °C), presented in Figure 3b, comprise two emission bands at around 1.25 and 1.55 μm. Due to the mentioned energy transfer between ions, the increase of Er^{3+} concentration quenched the Ni^{2+} emission intensity (Figure S5). Hence, the Er^{3+} content was selected to obtain emission spectra with comparable emission intensities of both $^3T_{2g}(F) \rightarrow {}^3A_{2g}(F)$ and $^4I_{13/2} \rightarrow {}^4I_{15/2}$ bands. The presence of Er^{3+} codoping has no an impact on the red shift of the Ni^{2+} emission band. To understand how temperature affects the emission of both Ni^{2+} and Er^{3+} ions in $SrTiO_3$ nanocrystals, the integrals of their emission intensities as a function of temperature are presented in Figure S6. Initially, at low temperatures up to −25 °C, intensities of both ions increase, however, in the case of Er^{3+} with a higher rate. This difference is related to the fact that the $Ni^{2+} \rightarrow Er^{3+}$ energy transfer increases the population of the $^4I_{13/2}$ state. Above 25 °C, rapid quenching of Ni^{2+} emission can be observed (reduction from 1.75 at −25 °C to 0.5 at 150 °C), while Er^{3+} intensity slightly decreases from 2.3 at −25 °C to 1.6 at 150 °C. This difference in the thermal dependence of the emission intensity of particular ions confirms that although the $Ni^{2+} \rightarrow Er^{3+}$ energy transfer plays a dominant role in the population of Er^{3+} excited states their emission intensity ratio can be used as a temperature-dependent parameter in luminescence thermometry. To quantify temperature-dependent changes in the emission intensity of Ni^{2+} and Er^{3+} ions, LIR is defined as follows

$$\mathrm{LIR}_2 = \frac{I_{Er^{3+}}}{I_{Ni^{2+}}} = \frac{\int I(1510-1580\ \mathrm{nm})}{\int I(1150-1200\ \mathrm{nm})} \quad (3)$$

For the calculation of Ni^{2+} integral intensity, the 1150−1200 nm spectral range was chosen. Choosing this spectral range

DOI: 10.1021/acs.jpcc.9b04002
J. Phys. Chem. C XXXX, XXX, XXX−XXX

Table 1. Comparison of Relative Sensitivities of Disparate Luminescent Thermometers Operating in II and III Optical Windows of Biological Tissues

host	dopants	S_R [%/°C]	temperature [°C]	references
Ag_2S		3−4	30	46
LaF_3	Er^{3+}, Yb^{3+}@Yb^{3+}, Tm^{3+}	3.5	30	47
PLGA HNS[a]	Nd^{3+}	2.5	30	19
$NaGdF_4$	Nd^{3+}, Er^{3+}, Ho^{3+}, Yb^{3+}	1	30	48
$SrTiO_3$	Ni^{2+}, Er^{3+}	0.76	30	this work
LaF_3	Yb@Nd	0.65	30	49
Y_2O_3	Nd^{3+}	0.43	30	50
LaF_3	Nd@Yb	0.41	10	49
YVO_4	Nd^{3+}	0.25	30	51
Gd_2O_3 (nanospheres)	Nd^{3+}	0.23	30	52
$KGd(WO_4)_2$	Nd^{3+}	0.16	30	53
Gd_2O_3 (nanorods)	Nd^{3+}	0.12	30	52
LaF_3	Nd^{3+}, Yb^{3+}	0.1	10	49

[a]$NaGdF_4$:Nd^{3+} NPs + PbS/CdS/ZnS QDs in a hybrid nanostructure (HNS) formed by poly(lactic-*co*-glycolic acid) (PLGA).

enables us to take advantage of both thermal quenching of Ni^{2+} ions emission intensity and the spectral shift of Ni^{2+} emission band maximum to enhance the value of the obtained relative sensitivity. Figures S7 and S8 present the results obtained for utilizing the whole Ni^{2+} emission band. Thermal evolution of the LIR_2 value for 0.05% Ni^{2+} and different concentrations of Er^{3+} is depicted in Figure 3c. It can be observed that a general tendency for all samples demonstrates a rise in the LIR_2 value with temperature, while relative changes of intensity decrease proportionally to the increase of Er^{3+} concentration. Additionally, for higher Er^{3+} concentrations, some fluctuation in the LIR_2 trend can be observed, which are caused by the small Ni^{2+} emission intensity for these nanocrystals. Observed differences in the thermal evolution rates of LIR_2 values for different Er^{3+} concentrations indicate that low Er^{3+} concentration is strongly desirable for a highly sensitive noncontact temperature readout in the II BW. The variation of relative sensitivity with temperature for different Er^{3+} concentrations is presented in Figure 3d. As can be clearly seen, the highest relative sensitivity was observed for the lowest dopant concentration. This tendency has been previously described for transition metal ions like Mn^{4+} or V^{5+}/V^{3+} and is probably related to the fact that for higher dopant concentrations the emission intensity is strongly quenched by the diffusion of the energy among excited states to the surface of the nanograin.[31,34] This efficient quenching channel suppresses the changes of the intensity related to the change of temperature. The fact that the highest values of the relative sensitivity were observed at the highest temperatures is caused by the strong quenching of Ni^{2+} emission in this temperature range. The maximal relative sensitivity in the biological temperature range was found to be S_R = 0.80%/°C at 45 °C for $SrTiO_3$:0.05% Ni^{2+};0.1% Er^{3+} (Figure 3d). On the other hand, the increase of the grain size of the nanoparticles causes reduction of the quenching rate of LIR and as a consequence of the relative sensitivity (Figure 3e,f). This effect may be explained by the stronger impact of the surface-related nonradiative processes, in the case of smaller nanoparticles, which affect the thermal quenching rate of the optically active ions. The performed analysis indicates that the most desirable feature for highly sensitive luminescent temperature sensing is possessing the $SrTiO_3$:Ni^{2+},Er^{3+} luminescent thermometer of the smallest grain size with the lowest concentration of Er^{3+} ions. However, it needs to be mentioned here that the integral emission intensity drops down when the size of the nanoparticles decreases. Therefore, depending on the application, the balance between the emission intensity and the relative sensitivity needs to be found. A comparison of the relative sensitivities obtained for different luminescent thermometers emitting in II OW, reported so far, is presented in Table 1. From this comparison, it can be deduced that the described material possess relatively higher sensitivity than most of the lanthanide-doped nanocrystals. We believe that by optimization of the host material, a further enhancement of S_R of Ni^{2+} nanocrystalline luminescent thermometers can be obtained. To the best of our knowledge, this is the first work introducing nanothermometry based on luminescence of both lanthanide and transition metal ions in the spectral range of II BW.

CONCLUSIONS

In this work, the first luminescent nanothermometer emitting in II OW based on luminescence of both lanthanide metal ions and transition metal ions was proposed. For this purpose, a series of $SrTiO_3$:Ni^{2+},Er^{3+} nanocrystalline powders with different concentrations of Ni^{2+} and Er^{3+} ions were successfully synthesized by the modified Pechini method. To fully understand luminescence properties of $SrTiO_3$:Ni^{2+},Er^{3+} nanocrystals, a thorough spectral analysis of obtained samples was conducted, namely, measurements of absorption, excitation, and emission spectra, the latter as a function of temperature over a wide temperature range (−150 to 210 °C). Spectroscopic properties of obtained $SrTiO_3$:Ni^{2+},Er^{3+} nanocrystals were investigated under 375 nm excitation, which was chosen to effectively excite both ions. However, it was found that a population of the $^4S_{3/2}$ energy state of Er^{3+} is mainly generated by an excessive energy transfer from the $^3T_{1g}(F)$ state of Ni^{2+} to the $^4S_{3/2}$ state of Er^{3+} and then a nonradiative depopulation to the $^4S_{3/2}$ energy state. Ni^{2+} ions provide strong and broadband emission centered at around 1.25 μm, ascribed to the $^3T_{2g}(^3F) \rightarrow {}^3A_{2g}(^3F)$ electron transition, which is highly susceptible to temperature changes, with a total suppression of the emission band at 210 °C. Moreover, a significant shift of the Ni^{2+} emission band toward longer wavelengths with increasing temperatures was observed, namely, 80 nm for −150 to 150 °C temperature range. The emission band of Er^{3+} ions is situated at around 1.55 μm, and its position remains stable with the temperature change. The luminescence intensity ratio of the luminescent nanothermometer based on

DOI: 10.1021/acs.jpcc.9b04002
J. Phys. Chem. C XXXX, XXX, XXX−XXX

emission bands of these two ions is defined as LIR = $I_{Er^{3+}}/I_{Ni^{2+}}$ = $\int I(1510-1580\ nm)/\int I(1150-1200\ nm)$. A general tendency of the increase in the LIR value with the increasing temperature was observed, while relative LIR values decreased with the Er^{3+} concentration. Due to the energy transfer occurring between Ni^{2+} and Er^{3+} ions, Er^{3+} emission is strongly dependent on Ni^{2+}, causing a rise of its thermal susceptibility and therefore resulting in lower sensitivity for such luminescent nanothermometer. The highest obtained values of sensitivity, in the biological temperature range (30−45 °C) was calculated to be 0.80%/°C; however, much higher values of sensitivity were demonstrated at higher temperatures, namely, 5.8%/°C at 150 °C. To sum up, aforementioned results demonstrate applicative potential of the $SrTiO_3$:Ni^{2+},Er^{3+} luminescent nanothermometer for biomedical purposes as well as unprecedented opportunities for further development in this field.

■ ASSOCIATED CONTENT

Supporting Information

The Supporting Information is available free of charge on the ACS Publications website at DOI: 10.1021/acs.jpcc.9b04002.

X-ray diffraction patterns and excitation spectra of $SrTiO_3$:Ni^{2+},Er^{3+} nanocrystals; activation energy calculations; LIR values and relative sensitivity as a function of temperature for $SrTiO_3$:0.1% Ni^{2+} spectral-shift luminescent nanothermometer; normalized emission spectra of $SrTiO_3$:Ni^{2+},Er^{3+} nanocrystals for different Er^{3+} concentrations; comparison of the integral intensities of Ni^{2+} ions and Er^{3+} ions for $SrTiO_3$:0.05% Ni^{2+},0.1% Er^{3+}; and normalized integral intensity and relative sensitivity of $SrTiO_3$:0.05% Ni^{2+},Er^{3+} calculated for the whole Ni^{2+} emission band (PDF)

■ AUTHOR INFORMATION

Corresponding Author

*E-mail: l.marciniak@intibs.pl.

ORCID

L. Marciniak: 0000-0001-5181-5865

Notes

The authors declare no competing financial interest.

■ ACKNOWLEDGMENTS

The "Highly sensitive thermal imaging for biomedical and microelectronic application" project is carried out within the First Team program of the Foundation for Polish Science co-financed by the European Union under the European Regional Development Fund.

■ REFERENCES

(1) Zohar, O.; Ikeda, M.; Shinagawa, H.; Inoue, H.; Nakamura, H.; Elbaum, D.; Alkon, D. L.; Yoshioka, T. Thermal Imaging of Receptor-Activated Heat Production in Single Cells. *Biophys. J.* **1998**, *74*, 82−89.

(2) Tardieu, F.; Reymond, M.; Hamard, P.; Granier, C.; Muller, B. Spatial Distributions of Expansion Rate, Cell Division Rate and Cell Size in Maize Leaves: A Synthesis of the Effects of Soil Water Status, Evaporative Demand and Temperature. *J. Exp. Bot.* **2000**, *51*, 1505−1514.

(3) Dramicanin, M. Biomedical Applications of Luminescence Thermometry. *Lumin. Nanothermometry* **2018**, 235−250.

(4) Jaque, D.; Vetrone, F. Luminescence Nanothermometry. *Nanoscale* **2012**, *4*, 4301−4326.

(5) del Rosal, B.; Ximendes, E.; Rocha, U.; Jaque, D. In Vivo Luminescence Nanothermometry: From Materials to Applications. *Adv. Opt. Mater.* **2017**, *5*, No. 1600508.

(6) Brites, C. D. S.; Lima, P. P.; Silva, N. J. O.; Millán, A.; Amaral, V. S.; Palacio, F.; Carlos, L. D. Thermometry at the Nanoscale. *Nanoscale* **2012**, *4*, 4799−4829.

(7) Dramićanin, M. D. Sensing Temperature via Downshifting Emissions of Lanthanide-Doped Metal Oxides and Salts. A Review. *Methods Appl. Fluoresc.* **2016**, *4*, No. 042001.

(8) Sordillo, D. C.; Sordillo, L. A.; Sordillo, P. P.; Alfano, R. R. Fourth Near-Infrared Optical Window for Assessment of Bone and Other Tissues. *Photonic Ther. Diagn. XII* **2016**, *9689*, No. 96894J.

(9) Welsher, K.; Sherlock, S. P.; Dai, H. Deep-Tissue Anatomical Imaging of Mice Using Carbon Nanotube Fluorophores in the Second near-Infrared Window. *Proc. Natl. Acad. Sci. U.S.A.* **2011**, *108*, 8943−8948.

(10) Kamimura, S.; Xu, C.-N.; Yamada, H.; Marriott, G.; Hyodo, K.; Ohno, T. Near-Infrared Luminescence from Double-Perovskite $Sr_3Sn_2O_7$:Nd^{3+}: A New Class of Probe for in Vivo Imaging in the Second Optical Window of Biological Tissue. *J. Ceram. Soc. Jpn.* **2017**, *125*, 591−595.

(11) Marciniak, L.; Bednarkiewicz, A.; Kowalska, D.; Strek, W. A New Generation of Highly Sensitive Luminescent Thermometers Operating in the Optical Window of Biological Tissues. *J. Mater. Chem. C* **2016**, *4*, 5559−5563.

(12) Marciniak, L.; Bednarkiewicz, A. Nanocrystalline NIR-to-NIR Luminescent Thermometer Based on Cr^{3+},Yb^{3+} Emission. *Sens. Actuators, B* **2017**, *243*, 388−393.

(13) Smith, A. M.; Mancini, M. C.; Nie, S. Bioimaging: Second Window for in Vivo Imaging. *Nat. Nanotechnol.* **2009**, *4*, 710−711.

(14) Sordillo, L. A.; Pu, Y.; Pratavieira, S.; Budansky, Y.; Alfano, R. R. Deep Optical Imaging of Tissue Using the Second and Third Near-Infrared Spectral Windows. *J. Biomed. Opt.* **2014**, *19*, No. 056004.

(15) Dramićanin, M. Chapter 6 − Lanthanide and Transition Metal Ion Doped Materials for Luminescence Temperature Sensing. *Lumin. Thermom.* **2018**, 113−157.

(16) Hernández-Rodríguez, M. A.; Lozano-Gorrín, A. D.; Martín, I. R.; Rodríguez-Mendoza, U. R.; Lavín, V. Comparison of the Sensitivity as Optical Temperature Sensor of Nano-Perovskite Doped with Nd^{3+} ions in the First and Second Biological Windows. *Sens. Actuators, B* **2018**, *255*, 970−976.

(17) Kolesnikov, I. E.; Kalinichev, A. A.; Kurochkin, M. A.; Golyeva, E. V.; Kolesnikov, E. Y.; Kurochkin, A. V.; Lähderanta, E.; Mikhailov, M. D. YVO_4:Nd^{3+} nanophosphors as NIR-to-NIR Thermal Sensors in Wide Temperature Range. *Sci. Rep.* **2017**, *7*, No. 18002.

(18) Wang, Z.; Jiao, H.; Fu, Z. Investigating the Luminescence Behaviors and Temperature Sensing Properties of Rare-Earth-Doped $Ba_2In_2O_5$ Phosphors. *Inorg. Chem.* **2018**, *57*, 8841−8849.

(19) Cerón, E. N.; Ortgies, D. H.; Del Rosal, B.; Ren, F.; Benayas, A.; Vetrone, F.; Ma, D.; Sanz-Rodríguez, F.; Solé, J. G.; Jaque, D.; et al. Hybrid Nanostructures for High-Sensitivity Luminescence Nanothermometry in the Second Biological Window. *Adv. Mater.* **2015**, *27*, 4781−4787.

(20) Ruiz, D.; del Rosal, B.; Acebron, M.; Palencia, C.; Sun, C.; Cabanillas-Gonzalez, J.; Lopez-Haro, M.; Hungria, A. B.; Jaque, D.; Juarez, B. H. Ag/Ag_2S Nanocrystals for High Sensitivity Near-Infrared Luminescence Nanothermometry. *Adv. Funct. Mater.* **2017**, *27*, No. 1604629.

(21) Wu, B.; Qiu, J.; Wu, E.; Zeng, H. Broadband Near-Infrared Luminescence from Transparent Glass-Ceramics Containing Ni^{2+}-Doped $SrTiO_3$ nanocrystals. *Opt. Mater.* **2013**, *35*, 983−987.

(22) Back, M.; Trave, E.; Ueda, J.; Tanabe, S. Ratiometric Optical Thermometer Based on Dual Near-Infrared Emission in Cr^{3+}-Doped Bismuth-Based Gallate Host. *Chem. Mater.* **2016**, *28*, 8347−8356.

(23) Chen, D.; Liu, S.; Xu, W.; Li, X. Yb^{3+}/Ln^{3+}/Cr^{3+} (Ln = Er, Ho) Doped Transparent Glass Ceramics: Crystallization, Ln $^{3+}$ Sensitized Cr^{3+} Upconversion Emission and Multi-Modal Temperature Sensing. *J. Mater. Chem. C* **2017**, *5*, 11769−11780.

DOI: 10.1021/acs.jpcc.9b04002
J. Phys. Chem. C XXXX, XXX, XXX−XXX

(24) Bednarkiewicz, A.; Trejgis, K.; Drabik, J.; Kowalczyk, A.; Marciniak, L. Phosphor-Assisted Temperature Sensing and Imaging Using Resonant and Nonresonant Photoexcitation Scheme. *ACS Appl. Mater. Interfaces* **2017**, *9*, 43081−43089.
(25) Elzbieciak, K.; Bednarkiewicz, A.; Marciniak, L. Temperature Sensitivity Modulation through Crystal Field Engineering in Ga^{3+} co-Doped $Gd_5Al_{5-x}Ga_xO_{12}:Cr^{3+}$, Nd3+nanothermometers. *Sens. Actuators, B* **2018**, *269*, 96−102.
(26) Elzbieciak, K.; Marciniak, L. The Impact of Cr^{3+} Doping on Temperature Sensitivity Modulation Co-Doped $Y_3Al_5O_{12}$, $Y_3Al_2Ga_3O_{12}$, $Y_3Ga_5O_{12}$ Nanothermometers. *Front. Chem.* **2018**, *6*, 424.
(27) Chen, D.; Xu, W.; Yuan, S.; Li, X.; Zhong, J. Ln^{3+}-Sensitized Mn^{4+} near-Infrared Upconverting Luminescence and Dual-Modal Temperature Sensing. *J. Mater. Chem. C* **2017**, *5*, 9619−9628.
(28) Chen, D.; Liu, S.; Zhou, Y.; Wan, Z.; Huang, P.; Ji, Z. Dual-Activator Luminescence of RE/TM: $Y_3Al_5O_{12}$ (RE = Eu^{3+}, Tb^{3+}, Dy^{3+}; TM = Mn^{4+}, Cr^{3+}) Phosphors for Self-Referencing Optical Thermometry. *J. Mater. Chem. C* **2016**, *4*, 9044−9051.
(29) Glais, E.; Dordević, V.; Papan, J.; Viana, B.; Dramićanin, M. D. $MgTiO_3:Mn^{4+}$ a Multi-Reading Temperature Nanoprobe. *RSC Adv.* **2018**, *8*, 18341−18346.
(30) Marciniak, L.; Trejgis, K. Luminescence Lifetime Thermometry with Mn^{3+} − Mn^{4+} Co-Doped Nanocrystals. *J. Mater. Chem. C* **2018**, *6*, 7092−7100.
(31) Trejgis, K.; Marciniak, L. The Influence of Manganese Concentration on the Sensitivity of Bandshape and Lifetime Luminescent Thermometers Based on $Y_3Al_5O_{12}:Mn^{3+}$, Mn^{4+}, Nd^{3+}nanocrystals. *Phys. Chem. Chem. Phys.* **2018**, *20*, 9574−9581.
(32) Gao, Y.; Cheng, Y.; Huang, F.; Lin, H.; Xu, J.; Wang, Y. Sn^{2+}/Mn^{2+} Codoped Strontium Phosphate ($Sr_2P_2O_7$) Phosphor for High Temperature Optical Thermometry. *J. Alloys Compd.* **2018**, *735*, 1546−1552.
(33) Kniec, K.; Marciniak, L. Spectroscopic Properties of $LaGaO_3:V,Nd^{3+}$ Nanocrystals as a Potential Luminescent Thermometer. *Phys. Chem. Chem. Phys.* **2018**, *20*, 21598−21606.
(34) Kniec, K.; Marciniak, L. The Influence of Grain Size and Vanadium Concentration on the Spectroscopic Properties of YAG:V^{3+},$V^{5+}$and YAG: V, Ln^{3+}(Ln^{3+} = Eu^{3+}, Dy^{3+}, Nd^{3+}) Nanocrystalline Luminescent Thermometers. *Sens. Actuators, B* **2018**, *264*, 382−390.
(35) Drabik, J.; Cichy, B.; Marciniak, L. New Type of Nanocrystalline Luminescent Thermometers Based on Ti^{3+}/Ti^{4+} and Ti^{4+}/Ln^{3+} (Ln^{3+} = Nd^{3+}, Eu^{3+}, Dy^{3+}) Luminescence Intensity Ratio. *J. Phys. Chem. C* **2018**, *122*, 14928−14936.
(36) Kobylinska, A.; Kniec, K.; Maciejewska, K.; Marciniak, L. The Influence of Dopant Concentration and Grain Size on the Ability to Temperature Sensing Using Nanocrystalline $MgAl_2O_4:Co^{2+}$, Nd^{3+} Luminescent Thermometers. *New J. Chem.* **2019**, 6080−6086.
(37) Bai, G.; Jie, W.; Yang, Z.; Hao, J. Temperature Dependence of Broadband Near-Infrared Luminescence from Ni^{2+}-Doped $Ba_{0.5}Sr_{0.5}TiO_3$. *J. Appl. Phys.* **2015**, *118*, No. 183110.
(38) Luitel, H. N.; Mizuno, S.; Takeda, Y. CaTiO3:Er3+,Ni2+broadband-Sensitive Upconverter: An Effective Way to Harvest Unused NIR Solar Irradiation for Crystalline Silicon Solar Cells. *Phys. Status Solidi A* **2017**, *214*, No. 1600899.
(39) Du, P.; Yu, J. S. Near-Ultraviolet Light Induced Visible Emissions in Er^{3+}-Activated La_2MoO_6 Nanoparticles for Solid-State Lighting and Non-Contact Thermometry. *Chem. Eng. J.* **2017**, *327*, 109−119.
(40) Du, P.; Yu, J. S. Near-Infrared Light-Triggered Visible Upconversion Emissions in Er^{3+}/Yb^{3+}-Codoped $Y_2Mo_4O_{15}$ Microparticles for Simultaneous Noncontact Optical Thermometry and Solid-State Lighting. *Ind. Eng. Chem. Res.* **2018**, *57*, 13077−13086.
(41) Du, P.; Yu, J. S. Synthesis of Er(III)/Yb(III)-Doped BiF_3 Upconversion Nanoparticles for Use in Optical Thermometry. *Microchim. Acta* **2018**, *185*, 237.
(42) Sunde, T. O. L.; Grande, T.; Einarsrud, M. A. Modified Pechini Synthesis of Oxide Powders and Thin Films. *Handb. Sol-Gel Sci. Technol.* **2018**, *0373*, 1089−1118.
(43) Long, J.; Yang, L.; Wei, X. Lattice, Elastic Properties and Debye Temperatures of $ATiO_3$ (A = Ba, Ca, Pb, Sr) from First-Principles. *J. Alloys Compd.* **2013**, *549*, 336−340.
(44) Scott, J. F. Self Mode Spectroscopy-Studies of Structural Phase Transitions. *Rev. Mod. Phys.* **1974**, *46*, 83−128.
(45) https://www.webelements.com/ (accessed June 05, 2019).
(46) Santos, H. D. A.; Ruiz, D.; Lifante, G.; Jacinto, C.; Juarez, B. H.; Jaque, D. Time Resolved Spectroscopy of Infrared Emitting Ag_2S Nanocrystals for Subcutaneous Thermometry. *Nanoscale* **2017**, *9*, 2505−2513.
(47) Ximendes, E. C.; Rocha, U.; Sales, T. O.; Fernández, N.; Sanz-Rodríguez, F.; Martín, I. R.; Jacinto, C.; Jaque, D. In Vivo Subcutaneous Thermal Video Recording by Supersensitive Infrared Nanothermometers. *Adv. Funct. Mater.* **2017**, *27*, No. 1702249.
(48) Skripka, A.; Benayas, A.; Marin, R.; Canton, P.; Hemmer, E.; Vetrone, F. Double Rare-Earth Nanothermometer in Aqueous Media: Opening the Third Optical Transparency Window to Temperature Sensing. *Nanoscale* **2017**, *9*, 3079−3085.
(49) Ximendes, E. C.; Santos, W. Q.; Rocha, U.; Kagola, U. K.; Sanz-Rodríguez, F.; Fernández, N.; Gouveia-Neto, A. D. S.; Bravo, D.; Domingo, A. M.; Del Rosal, B.; et al. Unveiling in Vivo Subcutaneous Thermal Dynamics by Infrared Luminescent Nanothermometers. *Nano Lett.* **2016**, *16*, 1695−1703.
(50) Kolesnikov, I. E.; Kalinichev, A. A.; Kurochkin, M. A.; Mamonova, D. V.; Kolesnikov, E. Y.; Kurochkin, A. V.; Lähderanta, E.; Mikhailov, M. D. $Y_2O_3:Nd^{3+}$ Nanocrystals as Ratiometric Luminescence Thermal Sensors Operating in the Optical Windows of Biological Tissues. *J. Lumin.* **2018**, *204*, 506−512.
(51) Kolesnikov, I. E.; Kalinichev, A. A.; Kurochkin, M. A.; Mamonova, D. V.; Kolesnikov, E. Y.; Kurochkin, A. V.; Lähderanta, E.; Mikhailov, M. D. New Strategy for Thermal Sensitivity Enhancement of Nd^{3+}-Based Ratiometric Luminescence Thermometers. *J. Lumin.* **2017**, *192*, 40−46.
(52) Balabhadra, S.; Debasu, M. L.; Brites, C. D. S.; Rocha, J.; Carlos, L. D. Implementing Luminescence Thermometry at 1.3 μm Using $(GdNd)_2O_3$nanoparticles. *J. Lumin.* **2016**, *180*, 25−30.
(53) Savchuk, O.; Carvajal, J. J.; De La Cruz, L. G.; Haro-González, P.; Aguiló, M.; Díaz, F. Luminescence Thermometry and Imaging in the Second Biological Window at High Penetration Depth with $Nd:KGd(WO_4)_2$ nanoparticles. *J. Mater. Chem. C* **2016**, *4*, 7397−7405.

DOI: 10.1021/acs.jpcc.9b04002
J. Phys. Chem. C XXXX, XXX, XXX−XXX